Vol. 24 • No. 6 • February 7 • 2012

D10488

www.advmat.de

ADVANCED MATERIALS

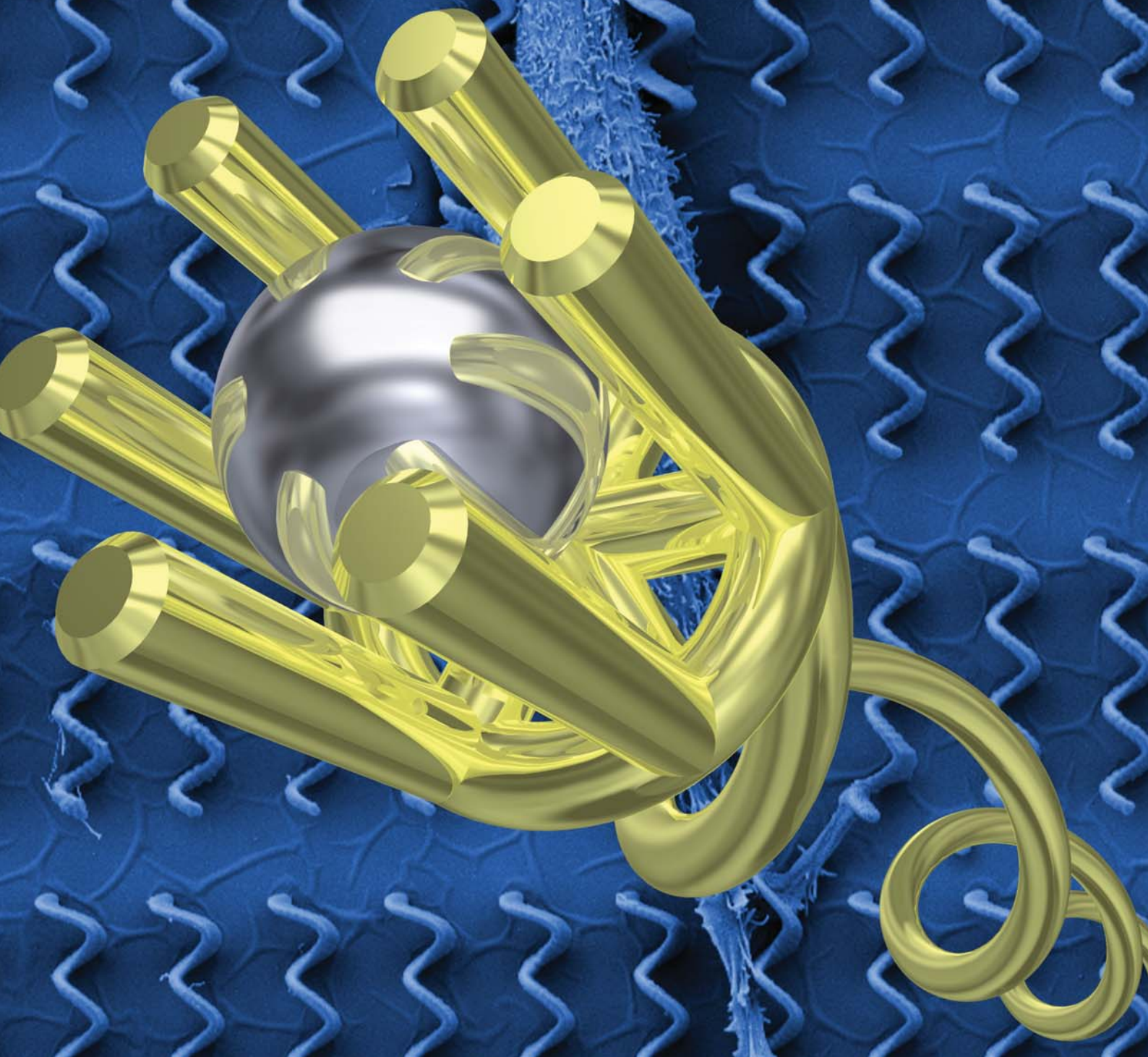

WILEY-VCH

Magnetic Helical Micromachines: Fabrication, Controlled Swimming, and Cargo Transport

Soichiro Tottori, Li Zhang, Famin Qiu, Krzysztof K. Krawczyk, Alfredo Franco-Obregón, and Bradley J. Nelson*

Rotation is a fundamental mechanical motion and is crucial for biological and artificial systems at the micro-/nanoscale. In nature, biomolecular rotary motors drive bacterial flagella and ATP synthase.[1–3] Inspired by such rotary motors, various micro-/nanorotors have been developed,[4] including chemical- and light-driven artificial molecular rotors,[2,5] electric-field-driven DNA nanorotors,[6] chemical-fuel-driven catalytic micro-/nanorotors,[7–9] and electric-field-driven CNT-based NEMS.[10] A rotating magnetic field has also been used to rotate a variety of magnetic micro/nano-scale objects, such as single/self-assembled beads,[11–15] rigid[16,17] and flexible wires,[18] and helical structures,[19,20] in fluid. Among these, helical micro-/nanoswimmers, inspired by bacterial flagella,[21] convert rotational motion to translational motion, which is one of the well-known propulsion strategies for a low Reynolds number regime.[22–24] They are capable of performing three-dimensional (3-D) swimming in liquid using a weak field without requiring a chemically modified environment. Because of these features, *in vivo* and micro/nanofluidic applications of helical micromachines have been proposed.[25,26] Helical microswimmers were recently fabricated using a "top-down" approach.[19] The swimmers consisted of soft-magnetic square "heads" and self-scrolled helical ribbon "tails".[27] Subsequently, smaller helical microswimmers were reported[20] using glancing angle deposition (GLAD).[28] The non-magnetic helical bodies were coated with a Co thin film, which was reported to be permanently magnetized by a strong magnetic field.

Here, we report a simple fabrication method of helical micromachines using 3-D direct laser writing (DLW)[29] and physical vapor deposition that allows us to design and fabricate helical devices of almost arbitrary shape with relative ease. These devices always generate corkscrew motion in fluid when the input frequency of the rotating field is sufficiently high. The helical micromachines exhibit excellent swimming performance in water and fetal bovine serum (FBS). We demonstrate cargo transport of microparticles in 3-D using a helical micromachine consisting of a helical body and a microholder. In comparison to previously reported helical microswimmers,[19,20] the targeted microobjects can be transported stably due to confinement[30] by the microholder.

The fabrication process is shown schematically in **Figure 1**a. The helical swimming micromachines were written in negative-tone photoresist (SU-8 or IP-L) by DLW (step 1). The unpolymerized photoresist was removed by a developer (step 2). After development and drying, Ni/Ti thin bilayers were deposited on the surface of the polymer helical micromachine by electron beam (e-beam) evaporation for magnetic actuation and improvement of surface biocompatibility (step 3). Two categories of shape designs were fabricated in the experiments. One has a bare helical shape and the other consists of a helical body and a microholder at one end. This illustrates a primary advantage of DLW, which provides the capability to create micromachines of various designs. The designs of some typical helical swimming machines are listed in **Table 1**. All helical micromachines in this paper have three turns and were fabricated with horizontal or vertical arrays.

Figure 1b shows the horizontal array of IP-L helical micromachines indicating that the fabrication process is highly reproducible. Each helical micromachine has a length of 8.8 μm and a diameter of 2.0 μm (Design VI in Table 1). The cross section of the filament is ellipsoidal with approximately 290 nm along the short axis and 900 nm along the long axis. Fabrication results showed that these helical structures were robust enough to remain stable while experiencing flow and surface tension during the development and drying processes and the subsequent e-beam evaporation process. The inset in Figure 1b shows a side view of helical structures before ferromagnetic thin film coating. Figure 1c shows a vertical helical micromachine from SU-8 (Design V in Table 1). The cross section of the filament was approximately 1.5 μm along the short axis and 2.9 μm along the long axis. Since the laser spot of DLW is elongated vertically (along the optical axis), the horizontal and vertical helices written by a single-line scanning are referred to as normal and binormal helices, respectively (see Figure S2 in Supporting Information). With multiple scanning lines, both types can be fabricated regardless of their orientation.

The orientation of the vertical helices can be changed during the fabrication process when their heights are larger than 22 μm. This is because the structures were pulled towards the substrate and the orientation became horizontal due to the flow they experienced during development and surface tension during drying. Despite these forces, the structures were robust enough to maintain their shape. The as-fabricated helical

S. Tottori, Dr. L. Zhang, F. Qiu, Prof. B. J. Nelson
Institute of Robotics and Intelligent Systems
ETH Zurich, Zurich, CH-8092, Switzerland
E-mail: lizhang@ethz.ch
S. Tottori
Department of Mechanical Engineering
University of Tokyo
7-3-1 Hongo Bunkyo, Tokyo, 113-8656, Japan
K. K. Krawczyk, Dr. A. Franco-Obregón
Space Biology Group, ETH Zurich, Zurich, CH-8005, Switzerland

DOI: 10.1002/adma.201103818

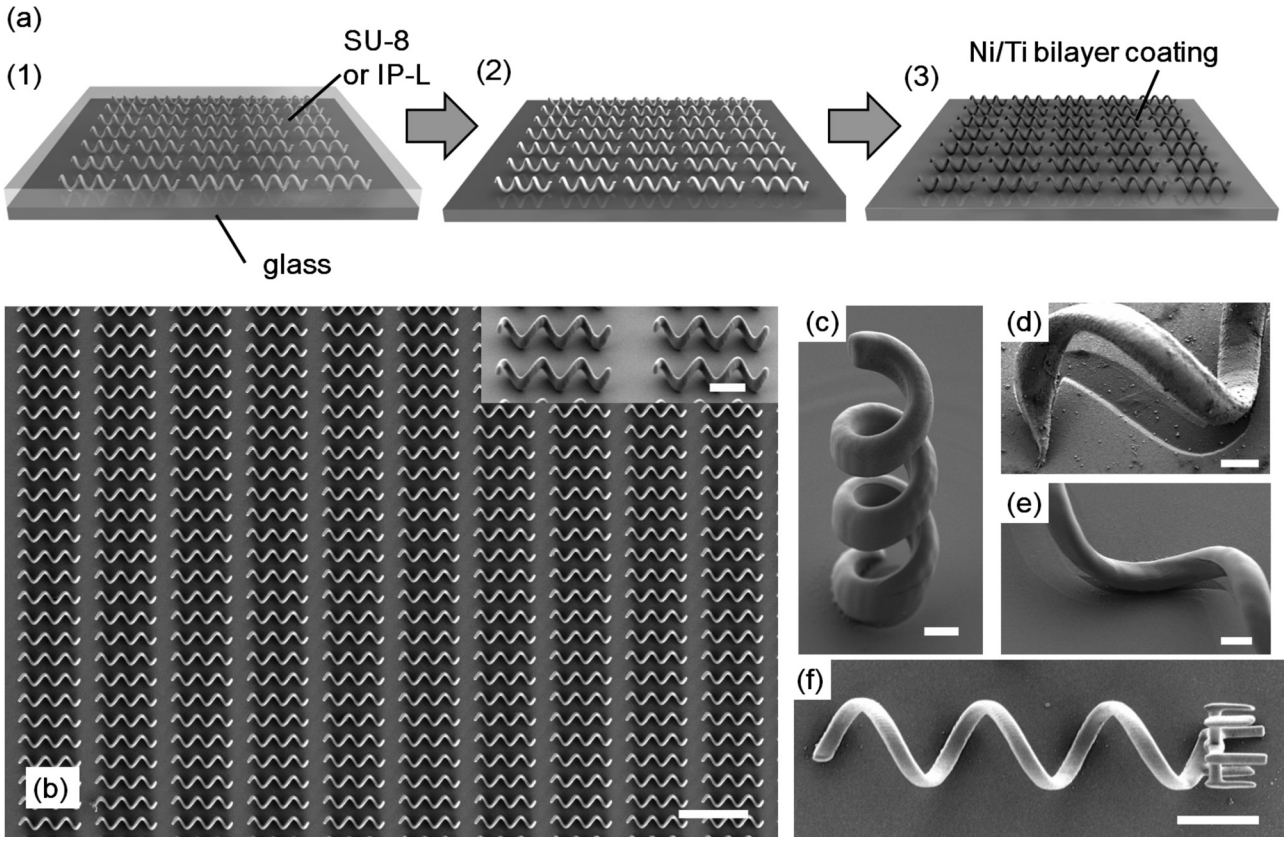

Figure 1. a) Fabrication procedure of helical swimming micromachines. b) A horizontal array of helical swimming micromachines from IP-L. The scale bars are 2 μm and 10 μm in the inset and overview, respectively. c) The vertical helical micromachine from SU-8. d) A strong shadowing effect was observed after the evaporation process with a tilt angle of 0°. e) The evaporation process was performed with a tilt angle of 15° to reduce shadowing. The scale bars in (c–e) are 2 μm. f) The helical micromachine with a microholder. The scale bar is 10 μm.

micromachines, horizontally laying on the glass substrate, were coated by Ni/Ti bilayers using e-beam evaporation. At a tilt angle of 0° a strong shadowing effect was observed in the evaporation process, as shown in Figure 1d, because the metal layers were evaporated vertically from the underlying metal sources. As the tilt angle was increased to 15°, the shadowing effect became insignificant, as shown in Figure 1e. For devices used in experiments, we selected a tilt angle of 15° for e-beam evaporation except for Design I in Table 1, which was evaporated with a tilt angle of 0°. Figure 1f shows a helical micromachine with a microholder consisting of six rigid finger-like protrusions (Design VIII). The inner diameter of the microholder was approximately 8.5 μm, and the diameter of the helical body was 10.0 μm. Other similar designs of microholders were also fabricated (see Figure S3 in Supporting Information).

In order to test for potential cytotoxic effects of the device surface treatments, the interaction between the fabricated devices and C2C12 mouse myoblasts were analyzed. For these studies the cells were cultured on substrates with both horizontal and vertical arrays of devices. **Figure 2**a–d shows SEM images of the interaction between the cells and the helical micromachines. These results verify that for both the horizontal (Figure 2a,b) and vertical (Figure 2c,d) arrays of helical micromachines prepared from IP-L and SU-8, respectively, the cells adhered well and extended apparently normal lamellipodia and filopodia over the surface of the devices. A comparison of cell proliferation on

Table 1. Design parameters of various helical swimming micromachines. The helix angle is defined as an angle between the tangent of the filaments and helical axis (Figure 3a inset).

Design	I	II	III	IV	V	VI	VII	VIII
Material	SU-8	SU-8	SU-8	SU-8	SU-8	IP-L	IP-L	SU-8
Length (μm)	35.0	64.5	47.3	39.0	21.9	8.8	4.0	57.0
Diameter (μm)	8.0	5.0	5.0	5.0	5.0	2.0	1.0	10.0
Helix angle	65°	35°	45°	50°	65°	65°	65°	66°
Ni/Ti thickness (nm)	100/–	100/5	100/5	100/5	100/5	50/5	50/5	100/5

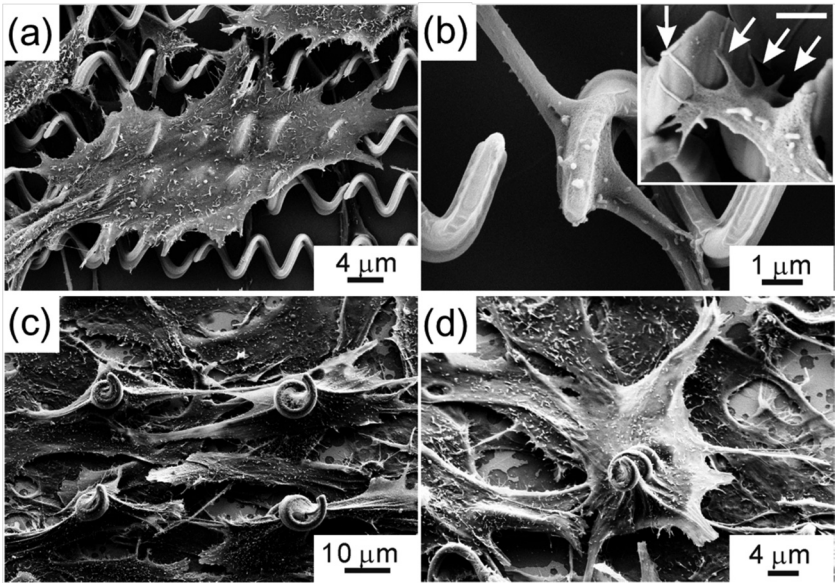

Figure 2. SEM microscopy images show cells rested on the horizontal array of IP-L helices (a,b) and vertical array of SU-8 helices (c,d) after 3-day culture, respectively. Inset: The SEM microscopy image shows that the helices were contacted by the lamellipodia and filopodia (indicated by white arrows) of the cell after a 1-day culture. The scale bar in the inset (b) is 1 μm.

untreated glass and two glass coverslips coated with the photoresists and Ni/Ti bilayers shows that the cells continued to proliferate on Ni/Ti bilayers after 72 hours of incubation (see Figure S5 in Supporting Information).

The magnetic shape anisotropy effect and the magnetic actuation of the magnetic helical devices were explored using a uniform static and rotating magnetic field, respectively. To characterize the behavior of helical micromachines in a static field, the helical micromachines with various helix angles ranging from 45° to 70° were suspended in deionized (DI) water and tested in a uniform field with a field strength of 5 mT. The plot in **Figure 3**a shows that the misalignment angle α decreased with a smaller helix angle θ. When the helix angle reached 45°, the misalignment angle was smaller than 10°. This tendency of the shape anisotropy effect can be explained by the fact that helical micromachines with small helix angles resemble rods or prolate ellipsoids, which align their longest axes to the direction of the external field. However, when the length to diameter ratio was smaller, i.e. with a large helix angle, the preferred direction of magnetization gradually changed to the radial axis of the helix. For instance, when the helix angle was 75°, the helical axis and the external field were almost perpendicular, i.e. 80°. We then applied a rotating magnetic field **B** with a frequency f. At relatively low frequencies the helical micromachines wobbled about their helical axes, shown schematically in Figure 3b. The wobbling angle β is defined as the angle between the rotational axis of a helix and its helical axis. As the input frequency increased, the wobbling angles gradually decreased and finally a corkscrew motion occurred, as shown in Figure 3c and 3d. When the applied field strength was increased, the applied frequency also had to be increased to induce a corkscrew motion. This is because the increasing field strength induced a larger torque that caused the helical axis to deviate from the rotating axis. The corresponding experimental results are shown in **Table 2**. Previously reported helical microswimmers with a thin Ni square plate as a "head" and a non-magnetic "tail," only wobbled at very low frequencies, i.e., below ~2 Hz at 2 mT. This was reported to be due to the unbalanced fluidic torque acting along the helical body.[31] The micromachines presented here required higher frequencies to realize corkscrew motions because they tend to be magnetized away from the radial axis of the helix. This is because the thin soft magnetic Ni film covers the entire helix instead of being concentrated at only a single more massive "head". The dynamics of the swimming results reveal that when a helical micromachine is rotated with a sufficiently high frequency, torques due to fluidic interactions can be utilized to eliminate the wobbling angle. The reduction of wobbling to a corkscrew motion was observed even at smaller

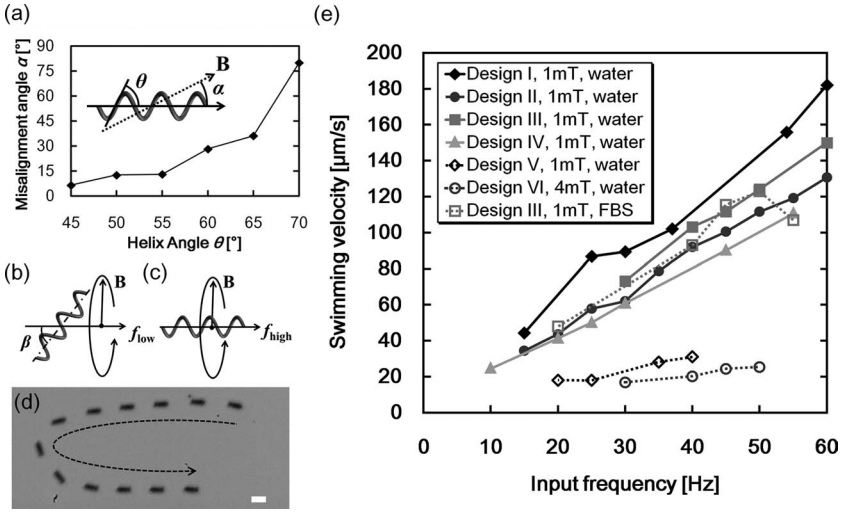

Figure 3. a) The misalignment angle α between the external field **B** and the helical axis as a function of various helix angles θ. b) Illustration of wobbling motion. A wobbling angle β is defined as an angle between the rotation axis and the helical axis. c) Illustration of corkscrew motion, at which a wobbling angle is negligibly small (see also Video S1 in the Supporting Information). d) The helical micromachine (Design VI in Table 1) was propelled with a corkscrew motion and precisely steered by changing the direction of the rotation axis (see also Video S2 in Supporting Information). The frequency and the strength of the field were 50 Hz and 4 mT, respectively. Time-lapse images were taken every 1 second. The scale bar is 10 μm. e) Average translational velocity plot for various geometrical designs of helical micromachines and fluid environments with respect to the input field frequency. Design I–VI correspond to the designs listed in Table 1.

Table 2. Stabilizing frequencies[32] that induced corkscrew motion in various strength fields for a helical micromachine with helix angle of 60° and diameter of 5.0 μm.

Field Strength [mT]	1	2	5	8
Stabilizing Frequency [Hz]	~15	~20	~35	~40

scales. The helical micromachines with Design VII were capable of performing corkscrew motion in a high-frequency rotating field, i.e. ~40 Hz at 1.5 mT. The helical micromachines that incorporated microholders, shown in Figure 1f (see also Figure S4 in the Supporting Information), were tested and all exhibited similar dynamics. Steering of the micromachines with or without microholders was possible with micrometer precision by simply changing the rotating axis of the field, an example of which is shown in Figure 3d.

The dependence of swimming velocity of various helical micromachines on their shape and size is presented in Figure 3e. The designs used in the plots are listed in Table 1. For all the plots, the linear relations between the swimming velocities and input frequencies were observed below the step-out frequencies.[33] In comparison with the three micromachines that have the same helix angle of 65° (Design I, V and VI), the one having the largest diameter, i.e. 8.0 μm (Design I) showed the highest speed, because the velocity U is proportional to the characteristic length:[34,35]

$$U = \frac{(C_n - C_l)\sin\theta\cos\theta}{2(C_n\sin^2\theta + C_l\cos^2\theta)} d\varpi \quad (1)$$

where C_n and C_l are the drag coefficients perpendicular and parallel to the filament, and d and ω are the diameter of the helix and the rotational frequency, respectively. With the same diameter of 5.0 μm (Design II, III, IV and V), the micromachine with a 45° helix angle (Design III) shows the highest swimming velocity, which is consistent with previous theoretical calculations.[35] The swimming behavior of one helical micromachine (Design III) was also tested in FBS as shown in Figure 3e. The step-out frequency of the micromachine was 55 Hz, lower than that in water due to the higher viscosity. However, the swimming speed in DI water and FBS was similar for the same input frequencies, which implies that the viscosity did not play a significant role for the velocity-frequency relation below the step-out frequencies. Equation 1 shows that the viscosity term is cancelled and does not change the slopes of U/ω. With the highest swimming speed achieved, i.e., 320 μm s^{-1} (9.1 body lengths per second) with Design I and 127 μm s^{-1} (14.4 body lengths per second) with Design VI (see Video S3 in Supporting Information), they can still be precisely steered. The conversion ratio of the translational distance per rotation normalized by a pitch length ranged approximately from 0.1 to 0.3 in our experiments.

Transportation of colloidal microparticles in 3-D was demonstrated using individual helical micromachines with a microholder fabricated together with the helical body. The procedure of targeted cargo transport can be separated into four stages: i) approaching, ii) loading, iii–iv) transporting in 2-D and 3-D, and v) releasing, as illustrated in **Figure 4**a. Figure 4b shows a time-lapse image of cargo transport of a 6-μm-diameter

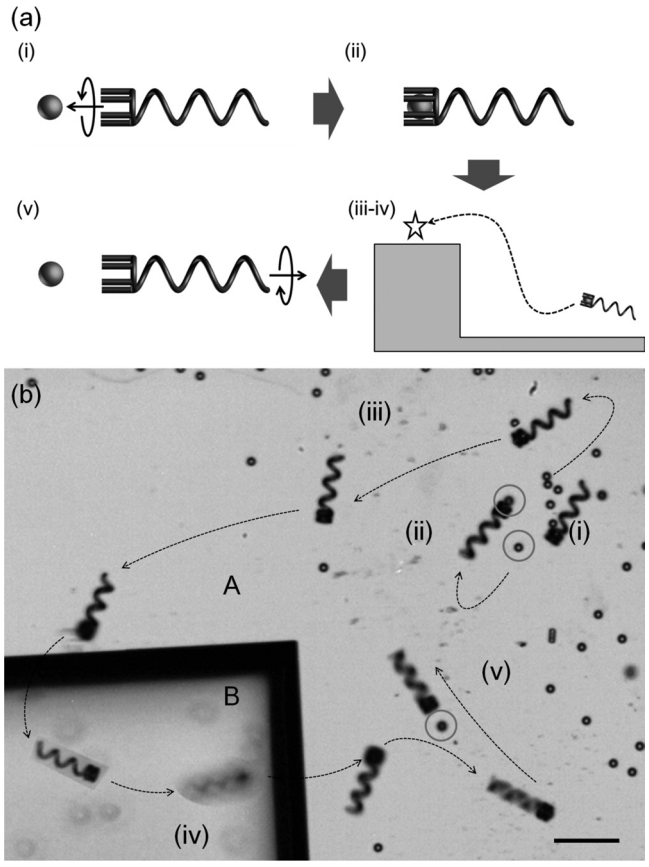

Figure 4. a) Illustration of transportation procedure by a helical micomachine with a microholder. b) Time-lapse image of the pick-and-place micromanipulation of a 6 μm diameter microparticle (see also Video S4 in the Supporting Information). The circles indicate the selected microparticle. The scale bar is 50 μm.

polystyrene (PS) particle in DI water that was initially lying on a patterned Si substrate. The helical micromachine first navigated towards the selected microparticle, noted as (i) in Figure 4b. In order to grasp the single microparticle, the micromachine was controlled to swim slightly downward with a small angle of attack, because the microbead was lying on the substrate. In (ii) the microparticle slipped into the microholder due to the confinement of the substrate and the fluidic drag applied on the microbead against the swimming direction. The microparticle was then transported over surface "A" and steered to the lower surface "B". Because of the forward motion of the helical micromachine and the lateral confinement from the six protrusions, the microparticle was stably transported without being dislodged even when traversing surfaces of different heights (see (iii) in Figure 4b). In order to transport the microparticle back to the higher surface "A," the micromachine was steered upwards and swam over the step, noted as (iv) in Figure 4b. Finally, micromachine rotation was reversed resulting in backward motion, and the microparticle was released from the front opening of the microholder, shown as (v) in Figure 4b. The microparticle was dragged for a short distance during the release because of localized flow generated by the microholder. By changing the size and shape of the

holder, micro- and nanoobjects of different sizes and shapes can be transported.[36,37]

In conclusion, we have demonstrated a simple and general approach for fabricating magnetic helical micromachines using 3-D laser writing and e-beam evaporation. The materials comprising the devices were not cytotoxic to mouse myoblasts, and the cells readily adhered, migrated and proliferated over the devices. These helical micromachines are capable of performing steerable corkscrew motion with a high speed in DI water and FBS as well as transport cargo in three dimensions. Because of the flexibility that direct laser writing coupled with conventional thin film evaporation provides to the fabrication process, a variety of swimming micromachines with various functional units can be fabricated using the method. These helical micromachines are promising for micromanipulation of biological samples and have potential for *in vivo* applications such as localized drug delivery.

Experimental Section

DLW of Helical Swimming Micromachines: Two different processes were developed to make devices of either SU-8 or IP-L. SU-8 (from Microchem) was first spin-coated on a glass substrate at 2000-3000 rpm for 30 s followed by a soft bake process using a hot plate at 95 °C for 15–30 minutes. For the second type of device, IP-L (from Nanoscribe GmbH) was coated on the glass substrate by a droplet. The 3-D structures were then written in either of the two photoresists using a Nanoscribe (from Nanoscribe GmbH) with the oil-immersion 100x objective (NA = 1.4 from Zeiss, NA denotes numerical aperture). The laser power and scan-speed for SU-8 and IP-L were 0.8 mW and 25 μm s^{-1}, and 2 mW and 25 μm s^{-1}, respectively. For SU-8, after a post exposure bake the substrate was developed in 1-methoxy-2-propanol-acetate (PGMEA) for 6–10 minutes and rinsed with isopropyl alcohol (IPA). The substrate coated with a droplet of IP-L was developed with IPA for 20 minutes and rinsed with fresh IPA without a post-bake. The substrate was then dried with nitrogen gas. To enhance the mechanical stability and adhesion to the glass substrate, individual helical filaments prepared from SU-8 were written by seven laser scans at a distance of 150 nm between the adjacent lines. The line distance was optimized to guarantee that each exposed line merged to form a single polymerized filament. In order to make the filaments thin, helical micromachines were also prepared by single line laser scanning in IP-L. Vertical arrays were prepared for the SU-8 helical micromachines, and IP-L arrays were prepared horizontally in order to avoid collapse of the helical structures due to surface tension during the drying process. Exposure dose tests based on straight-line laser scans were conducted to evaluate the resolution and shape of the filament (see Figure S1 in Supporting Information).

E-Beam Evaporation of Ni/Ti Bilayers: The developed glass substrates were evaporated with Ni/Ti bilayer by an e-beam evaporator (Plassys-II MEB550SL) with a rotational speed of 4–10 rpm, and tilt angles of 0° and 15° were tested. The deposition rate of Ni and Ti films was 0.2 nm s^{-1}.

Supporting Information

Supporting Information is available from the Wiley Online Library or from the author.

Acknowledgements

We thank the FIRST lab of ETH Zurich for technical support. The authors are also grateful to Dr. Bradley Kratochvil (ETH Zurich) for providing technical support of the experimental setup, Ruedi Borer (ETH Zurich) for the construction of the power amplifier for the Helmholtz coils setup, Klaus Marquardt (University of Zurich) for help of the samples preparation for SEM inspection of cells, Kathrin Peyer (ETH Zurich) for fruitful discussions and Erdem Siringil (ETH Zurich) for help with the experimental setup. Funding for this research was partially provided by the European Research Council Advanced Grant "Microrobotics and Nanomedicine (BOTMED)".

Received: October 5, 2011
Revised: November 25, 2011
Published online: January 2, 2012

[1] K. Kinbara, T. Aida, *Chem. Rev.* **2005**, *105*, 1377.
[2] R. Eelkema, M. M. Pollard, J. Vicario, N. Katsonis, B. S. Ramon, C. W. M. Bastiaansen, D. J. Broer, B. L. Feringa, *Nature* **2006**, *440*, 163.
[3] M. G. L. van den Heuvel, C. Dekker, *Science* **2007**, *317*, 333.
[4] G. A. Ozin, I. Manners, S. Fournier-Bidoz, A. Arsenault, *Adv. Mater.* **2005**, *17*, 3011.
[5] S. P. Fletcher, F. Dumur, M. M. Pollard, B. L. Feringa, *Science* **2005**, *310*, 80.
[6] Y. Klapper, N. Sinha, T. W. S. Ng, D. Lubrich, *Small* **2010**, *6*, 44.
[7] S. Fournier-Bidoz, A. C. Arsenault, I. Manners, G. A. Ozin, *Chem. Commun.* **2005**, 441.
[8] Y. Wang, S. T. Fei, Y. M. Byun, P. E. Lammert, V. H. Crespi, A. Sen, T. E. Mallouk, *J. Am. Chem. Soc.* **2009**, *131*, 9926.
[9] A. A. Solovev, Y. F. Mei, O. G. Schmidt, *Adv. Mater.* **2010**, *22*, 4340.
[10] A. M. Fennimore, T. D. Yuzvinsky, W. Q. Han, M. S. Fuhrer, J. Cumings, A. Zettl, *Nature* **2003**, *424*, 408.
[11] T. R. Strick, V. Croquette, D. Bensimon, *Nature* **2000**, *404*, 901.
[12] I. Petousis, E. Homburg, R. Derks, A. Dietzel, *Lab Chip* **2007**, *7*, 1746.
[13] P. Tierno, R. Golestanian, I. Pagonabarraga, F. Sagues, *Phys. Rev. Lett.* **2008**, *101*, 218304.
[14] C. E. Sing, L. Schmid, M. F. Schneider, T. Franke, A. Alexander-Katz, *Proc. Nat. Acad. Sci. USA* **2010**, *107*, 535.
[15] O. Guell, F. Sagues, P. Tierno, *Adv. Mater.* **2011**, *23*, 3674.
[16] P. Dhar, C. D. Swayne, T. M. Fischer, T. Kline, A. Sen, *Nano Lett.* **2007**, *7*, 1010.
[17] L. Zhang, T. Petit, Y. Lu, B. E. Kratochvil, K. E. Peyer, R. Pei, J. Lou, B. J. Nelson, *ACS Nano* **2010**, *4*, 6228.
[18] W. Gao, S. Sattayasamitsathit, K. M. Manesh, D. Weihs, J. Wang, *J. Am. Chem. Soc.* **2010**, *132*, 14403.
[19] L. Zhang, J. J. Abbott, L. X. Dong, B. E. Kratochvil, D. Bell, B. J. Nelson, *Appl. Phys. Lett.* **2009**, *94*, 064107.
[20] A. Ghosh, P. Fischer, *Nano Lett.* **2009**, *9*, 2243.
[21] H. C. Berg, R. A. Anderson, *Nature* **1973**, *245*, 380.
[22] E. M. Purcell, *Am. J. Phys.* **1977**, *45*, 3.
[23] S. J. Ebbens, J. R. Howse, *Soft Matter* **2010**, *6*, 726.
[24] J. J. Abbott, K. E. Peyer, M. C. Lagomarsino, L. Zhang, L. X. Dong, I. K. Kaliakatsos, B. J. Nelson, *Int. J. Robot. Res.* **2009**, *28*, 1434.
[25] B. J. Nelson, I. K. Kaliakatsos, J. J. Abbott, *Annu. Rev. Biomed. Eng.* **2010**, *12*, 55.
[26] L. Zhang, K. E. Peyer, B. J. Nelson, *Lab Chip* **2010**, *10*, 2203.
[27] L. Zhang, L. X. Dong, D. J. Bell, B. J. Nelson, C. Schoenenberger, D. Gruetzmacher, *Microelectron. Eng.* **2006**, *83*, 1237.
[28] K. Robbie, M. J. Brett, A. Lakhtakia, *Nature* **1996**, *384*, 616.
[29] C. N. LaFratta, J. T. Fourkas, T. Baldacchini, R. A. Farrer, *Angew. Chem. Int. Ed.* **2007**, *46*, 6238.
[30] M. S. Sakar, E. B. Steager, D. H. Kim, M. J. Kim, G. J. Pappas, V. Kumar, *Appl. Phys. Lett.* **2010**, *96*, 043705.

[31] K. E. Peyer, L. Zhang, B. E. Kratochvil, B. J. Nelson, presented at *2010 IEEE Inter. Conf. Robotics and Automation (ICRA 2010)*, Anchorage, Alaska, May, **2010**.
[32] The stabilizing frequency is defined as the frequency at which the wobbling angle becomes less than ±5°.
[33] A step-out frequency is the frequency at which the helical micromachine starts to rotate asynchronously with an input rotating field.
[34] J. Gray, G. J. Hancock, *J. Exp. Biol.* **1955**, *32*, 802.
[35] E. Lauga, T. R. Powers, *Rep. Prog. Phys.* **2009**, *72*, 096601.
[36] J. S. Randhawa, T. G. Leong, N. Bassik, B. R. Benson, M. T. Jochmans, D. H. Gracias, *J. Am. Chem. Soc.* **2008**, *130*, 17238.
[37] J. S. Randhawa, M. D. Keung, P. Tyagi, D. H. Gracias, *Adv. Mater.* **2010**, *22*, 407.